Michler's hydrol blue elucidates structural differences in prion strains

Yiling Xiao[a], Sandra Rocha[b], Catherine C. Kitts[c], Anna Reymer[d], Tamás Beke-Somfai[e], Kendra K. Frederick[a,1], and Bengt Nordén[c,1]

[a]Department of Biophysics, University of Texas Southwestern Medical Center, Dallas, TX 75390-8816; [b]Department of Biology and Biological Engineering, Chalmers University of Technology, SE-412 96 Gothenburg, Sweden; [c]Department of Chemistry and Chemical Engineering, Chalmers University of Technology, SE-412 96 Gothenburg, Sweden; [d]Department of Chemistry and Molecular Biology, University of Gothenburg, SE-405 30 Gothenburg, Sweden; and [e]Institute of Materials and Environmental Chemistry, Research Centre for Natural Sciences, Hungarian Academy of Sciences, H-1117 Budapest, Hungary

Edited by William F. DeGrado, University of California, San Francisco, CA, and approved September 1, 2020 (received for review January 30, 2020)

Yeast prions provide self-templating protein-based mechanisms of inheritance whose conformational changes lead to the acquisition of diverse new phenotypes. The best studied of these is the prion domain (NM) of Sup35, which forms an amyloid that can adopt several distinct conformations (strains) that confer distinct phenotypes when introduced into cells that do not carry the prion. Classic dyes, such as thioflavin T and Congo red, exhibit large increases in fluorescence when bound to amyloids, but these dyes are not sensitive to local structural differences that distinguish amyloid strains. Here we describe the use of Michler's hydrol blue (MHB) to investigate fibrils formed by the weak and strong prion fibrils of Sup35NM and find that MHB differentiates between these two polymorphs. Quantum mechanical time-dependent density functional theory (TDDFT) calculations indicate that the fluorescence properties of amyloid-bound MHB can be correlated to the change of binding site polarity and that a tyrosine to phenylalanine substitution at a binding site could be detected. Through the use of site-specific mutants, we demonstrate that MHB is a site-specific environmentally sensitive probe that can provide structural details about amyloid fibrils and their polymorphs.

Sup35NM | amyloid fibril | prion | amyloid dye | fluorescence spectroscopy

Amyloids are unbranched fibrils of protein aggregates arranged as β-strands that run perpendicular to the fiber axis, forming a cross β-sheet of indefinite length (1–4). They are related to several common human diseases such as Alzheimer's disease and type II diabetes (4–7). Amyloids can also be beneficial, such as those found in yeast, where they can help cells survive environmental fluctuations (6, 8, 9). An important feature of amyloid fibrils is their polymorphism, which refers to structural variations in fibrils formed by a particular polypeptide chain under the same environmental conditions (2–4, 6, 10–16). In yeast, as well as in other organisms, polymorphisms are also referred to as strains because cells that harbor them have different phenotypes (17, 18). The yeast prion protein, Sup35, can adopt a variety of amyloid polymorphs, of which at least two, named "weak" and "strong," describe the phenotypes they confer in vivo (19). The amyloid core of the strong prion fibrils comprises the first 40 residues of Sup35, and the amyloid core of the weak prion fibrils comprises the first 70 residues (17, 20). These two polymorphs have tightly packed β-sheet-rich amyloid cores with distinct molecular structures (20, 21) that are protected from the outside environment. However, the location of the beta strands and turns for individual monomers of Sup35 when they are assembled into any amyloid form remains poorly defined since Sup35 amyloid fibers have highly degenerate sequences, making them difficult to study by solid-state NMR spectroscopy, and lack repeating structural features, making them difficult to study using cryo-electron microscopy.

The most commonly used probe to monitor amyloid fibril formation is still thioflavin T (ThT), a fluorescent molecular rotor discovered many decades ago (22–25). When bound to amyloid fibrils, molecular rotors become conformationally confined and experience an environment with different polarity compared to bulk water. The conformational restriction increases the quantum efficiency of the molecular rotors, making these dyes sensitive amyloid indicators and thus particularly suitable for amyloid fibril detection. However, the spectral properties of ThT, as well as other classic amyloid dyes such as Congo red, are not altered by changes in polarity, and thus, they do not distinguish between different amyloid polymorphs (26). Some more modern amyloid dyes, such as luminescent-conjugated polythiophenes, can distinguish between amyloid polymorphs; however, the resulting spectral changes cannot be directly attributed to any specific differences in the physiochemical properties of the different fibril structures (27–29). Michler's hydrol blue (MHB), a symmetric molecular rotor, binds to amyloid fibrils with high affinity, and the spectral properties of MHB are sensitive to local changes in hydrophobicity (30). MHB aligns parallel to the fiber at an angle of 14° to 22° to the axis along the grooves of the β-sheets and preferentially binds near aromatic rings (30). Quantum mechanical investigations explain this valuable property of MHB, and the related group of cationic tri- and diarylmethane dyes (31–34); the lowest excited state dynamics in the two lowest excited states of MHB are sensitive to the polarity of the local environment. As some of the features for MHB binding to amyloid fibers are defined and the spectral properties of the dye are dependent on the local environment, MHB could potentially be a structurally specific fluorescent probe.

Significance

Amyloids are protein fiber aggregates that are associated with both pathology, e.g., neurodegenerative diseases, and functionality, e.g., adaptation to environmental changes in yeasts. A particular property of amyloid fibrils is their ability to show structural variations among different fibrils formed by the same polypeptide chain, a phenomenon known as polymorphism. It is becoming increasingly important to be able to distinguish between amyloid polymorphs because they can cause pathologically distinct transmissible diseases. Here we describe a fluorescent amyloid dye that can differentiate between amyloid polymorphs.

Author contributions: K.K.F. and B.N. designed research; Y.X., S.R., C.C.K., A.R., T.B.-S., and K.K.F. performed research; Y.X., S.R., C.C.K., A.R., T.B.-S., K.K.F., and B.N. analyzed data; and S.R., T.B.-S., and K.K.F. wrote the paper.

The authors declare no competing interest.

This article is a PNAS Direct Submission.

[1]To whom correspondence may be addressed. Email: kendra.frederick@utsouthwestern.edu or norden@chalmers.se.

This article contains supporting information online at https://www.pnas.org/lookup/suppl/doi:10.1073/pnas.2001732117/-/DCSupplemental.

First published November 9, 2020.

In this work, we use fluorescence spectroscopy to monitor amyloid assembly using the molecular rotor dye MHB. We use computational simulations to determine whether and how the change in hydrophobicity associated with a tyrosine to phenylalanine mutation could alter the fluorescence properties of MHB. We test these predictions on a series of weak and strong prion fibrils harboring single tyrosine to phenylalanine mutations and report the excitation and emission spectra of MHB in the presence of Sup35NM in the weak and strong prion fibril conformations. We find that MHB displays different spectral shifts when bound to the strong and weak prions. Furthermore, the analysis of Sup35 mutants in which a tyrosine in the N-terminal region was replaced by phenylalanine shows that the probe can detect differences in the structure and polarity of the fibrils that can be localized to a specific residue.

Results

MHB Does Not Impede Amyloid Formation. Sup35NM aggregation follows a classical nucleation-dependent polymerization when amyloid formation is monitored by ThT (35, 36). The MHB fluorescence emission of Sup35NM assembly reactions was measured to determine whether MHB could be used to detect amyloid formation. Solutions of monomeric denatured Sup35NM were incubated in the presence of MHB, ThT, or both dyes, and the fluorescence emission was monitored. As seen for fibrils of other proteins (30), the fluorescence of MHB in the presence of amyloid fibril forms of the Sup35NM protein is two orders of magnitude higher than when it is in the presence of denatured monomeric species of Sup35NM. For unseeded reactions (Fig. 1*A*), the fluorescence readings for both dyes had distinct phases: a lag phase, an elongation phase, and a saturation phase. The lag phase can be bypassed by the addition of a small amount of premade amyloid fibrils, and the seeded elongation phases had different aggregation rates that depended upon the conformation and the amount of the amyloid seed that was introduced into the reaction (Fig. 1*B*). The lag phase, elongation phase, and saturation phase of Sup35NM amyloid formation were identical for reactions monitored by ThT and MHB fluorescence. Thus, we conclude that MHB, like ThT, does not affect the amyloid fibril formation of Sup35NM.

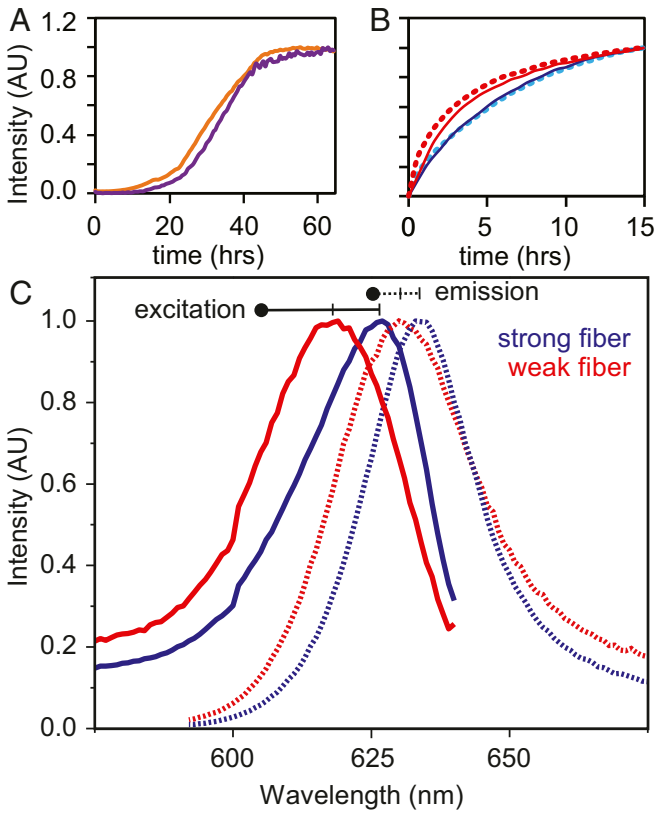

Fig. 1. (*A*) Unseeded amyloid fibril formation of Sup35NM monitored by fluorescence emission of ThT (orange) and MHB (purple). (*B*) Amyloid formation of Sup35NM seeded with weak prion fibrils (red) and strong prion fibrils (blue) monitored by ThT (dotted lines) and MHB (solid lines). Fluorescence intensities are plotted as normalized values. The unnormalized intensities are shown in *SI Appendix*, Fig. S1. (*C*) Fluorescence excitation (solid lines) and emission (dotted lines) spectra of MHB in the presence of weak prion fibrils (red) and strong prion fibrils (blue). The excitation and emission maxima of unbound MHB are indicated by black circles.

MHB Distinguishes between Different Conformers of the Same Protein. Prior work on model systems as well as computation revealed that the exposure of MHB to less polar environments resulted in progressively redshifted excitation and emission profiles (30). We therefore investigated whether MHB can distinguish between different amyloid conformations of the same protein. The excitation and emission spectra of MHB bound to strong and weak prion fibrils were collected. The excitation maximum of MHB in solution is centered at 605 nm, and the emission peaks at 625 nm (30). In the presence of weak prion fibrils, the excitation and emission maxima of MHB redshifted to 618 and 630 nm, respectively (Fig. 1*C*). In the presence of strong prion fibrils, the excitation and emission maxima of MHB had even more pronounced redshifts to 627 and 634 nm, respectively (Fig. 1*C*). The full width at half maximum (FWHM) of the excitation and emission spectra of MHB bound to strong prion fibrils narrowed by 3 and 8 nm, respectively, relative to the spectra of MHB bound to weak prion fibrils (*SI Appendix*, Table S1). The more pronounced shift to higher wavelengths in the MHB excitation spectrum and narrowing of the spectra observed for the strong strain indicate that strong prion fibrils are less polar than the weak prion fibrils. Differences in the excitation and emission spectra of MHB bound to amyloid fibrils of the same protein in different conformations demonstrate that MHB fluorescence is sensitive to and can distinguish between distinct polymorphs. The excitation and emission spectra of MHB acted as an indicator of conformational differences due to differences in polarity between weak and strong prion fibril conformations.

Theoretical Calculations Predict Redshift for Tyrosine to Phenylalanine Mutants. Weak and strong prion fibrils have different structures, and the fluorescence of MHB bound to the fibrils was sensitive to these structural differences. As prior work suggested that MHB binds to amyloid fibers near aromatic rings with defined orientations, we then analyzed whether very small, site-specific changes in polarity could affect the MHB. Mutation of a tyrosine to a phenylalanine residue replaces a hydroxyl at the para position of the aromatic ring with a hydrogen. We calculated whether the decrease in polarity that accompanies a tyrosine to phenylalanine substitution at the MHB binding site could be tracked when MHB binding is modeled on a β-sheet plateau. Quantum mechanical time-dependent density functional theory (TDDFT) calculations were performed by using models based on previous data obtained for MHB structure and orientation (30, 37) and by applying different levels of theory on MHB π-stacked to either tyrosine or phenylalanine. The resulting relative spectral properties were compared with four different combinations of quantum mechanical levels of theory (Fig. 2 and *SI Appendix*, Table S1). Each theoretical model indicated a slight redshift upon changing tyrosine to phenylalanine, with an average redshift of +0.9 nm. Thus, quantum mechanical TDDFT calculations predicted that a single tyrosine to phenylalanine change at a binding site for MHB should

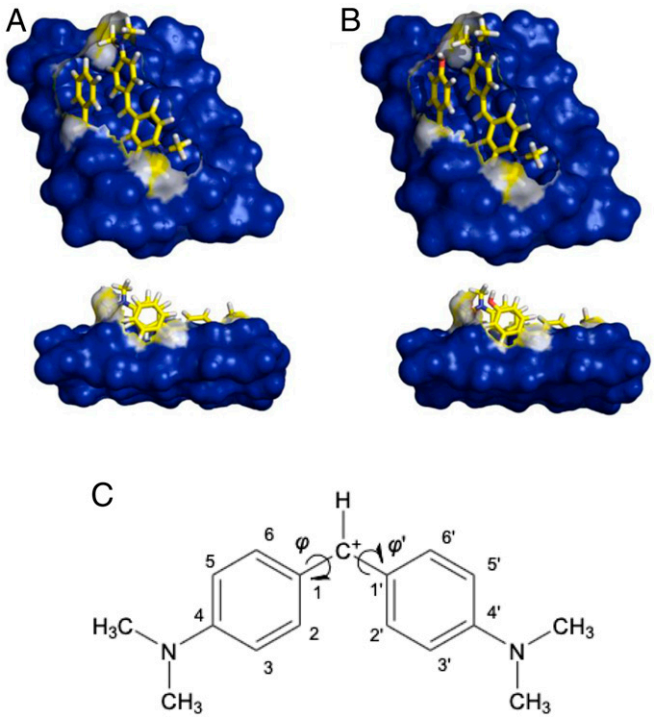

Fig. 2. Surface models of MHB bound on a β-sheet π-stacked to either F (*A*) or Y (*B*) optimized using the ONIOM [ωB97X-D/6-31G(d):PM3MM] approach. The antiparallel β-sheet is shown as van der Waals spheres, and the tyrosine and phenylalanine side chains, as well as MHB, are shown as yellow sticks. (*C*) Chemical structure and dihedral angles φ and φ′ of MHB.

result in shifts in the MHB excitation spectra. For more details see *SI Appendix*.

Substitution of Tyrosine by Phenylalanine Does Not Alter Templated Fibril Conformation. Our calculations suggested that a tyrosine (Y) to phenylalanine (F) substitution could alter the excitation and emission spectra of MHB. Tyrosine residues are located throughout the amyloid-forming region of Sup35NM. Therefore, specific tyrosine residues were mutated to phenylalanine to increase the hydrophobicity in a site-specific manner. We analyzed the thermal stability of weak and strong prion fibrils to confirm that tyrosine to phenylalanine substitutions do not alter the structure of fibrils (*SI Appendix*, Fig. S2 and Table S2). The melting temperatures obtained for each strain in the presence of sodium dodecyl sulphate confirmed that weak and strong prion fibrils have distinct resistance to thermal denaturation and thus markedly different physical properties. The weak prion fibrils formed by lysate-templated wild type (WT) Sup35NM monomers had a melting temperature of 74 ± 3 °C, while the melting temperature for the strong prion fibrils formed by lysate-templated WT Sup35NM monomers was significantly lower at 57 ± 6 °C. Solutions of purified, denatured Y→F mutants of Sup35NM were templated into the prion conformation by either weak or strong prion fibrils made from WT Sup35NM to determine whether the mutants could faithfully propagate the strains. The resulting mutant prion fibrils were, in turn, used to template purified denatured WT Sup35NM. The weak prion fibrils formed by mutant-fibril-templated WT Sup35NM monomers had a melting temperature of 72 ± 4 °C (average of all cases), while the melting temperature of the strong prion fibrils formed by mutant-fibril-templated WT Sup35NM monomers was significantly lower at 60 ± 5 °C (*SI Appendix*, Fig. S2). The melting temperatures of the mutant-templated WT Sup35NM fibrils were the same as the WT Sup35NM templated WT Sup35NM fibrils. While similarities in the melting temperatures cannot formally eliminate the possibility of small structural differences in the mutant prion fibrils, the similarities indicate that the weak and strong prion fibril conformations were faithfully propagated in the presence of tyrosine to phenylalanine mutations. Thus, any changes in the MHB excitation and emission spectra report on site-specific changes in hydrophobicity caused by the substitution of tyrosine with phenylalanine and not structural alterations of the amyloid fibrils due to mutations.

MHB Detects Site-Specific Changes in Polarity. We measured the excitation and emission spectra of MHB in the presence of weak and strong prion fibrils that carried a single Y→F mutation to determine whether MHB could detect site-specific changes in polarity. The excitation spectra of some, but not all, mutants were redshifted relative to the WT weak and strong prion fibrils, and these changes were consistent with known structural features of these polymorphs. The excitation spectra of MHB in the presence of weak prion fibrils of Sup35NM mutants Y16F, Y32F, Y35F, Y49F, and Y52F were redshifted by 4 to 6 nm relative to that of weak prion fibrils of WT Sup35NM (Fig. 3*A*). Moreover, the emission spectra of MHB bound to these mutants were redshifted on average 3 nm and the FWHM of the emission spectra narrowed by an average of 5 nm (Fig. 3*B*). MHB experienced a more nonpolar environment when bound to weak prion fibrils made from these individual tyrosine to phenylalanine mutants than when bound to weak prion fibrils of WT Sup35NM. The redshifting also indicates that these aromatic residues are located at the binding sites for MHB because changing a tyrosine to a phenylalanine makes the local environment in the β-sheet more nonpolar. In contrast, the excitation and emission spectra of MHB in the presence of weak prion fibrils of Sup35NM mutants Y13F, Y29F, Y45F, and Y69F were only very slightly shifted relative to the WT weak prion fibrils (Fig. 3 *E* and *F*). The FWHM for the emission spectra for these mutants narrowed by 2 nm, but the FWHM of the excitation broadened slightly. This indicates that MHB does not bind near amino acids Y13, Y29, Y45, or Y69 in the weak prion fibrils.

While the MHB excitation and emission spectra of strong prion fibrils of WT Sup35NM are overall significantly more redshifted than those of weak prion fibrils (Fig. 1*B*), the redshifts observed for MHB spectra in the presence of the strong prion fibril conformation of Y→F mutants are more modest and affect fewer sites. This result is consistent with fewer potential MHB binding sites in strong prion fibrils as their amyloid core is smaller than that of the weak prion fibrils. The excitation spectra of MHB in the presence of strong prion fibrils of Sup35NM of only two mutants, Y13F and Y32F, were redshifted by 1.5 nm relative to that of strong prion fibrils of WT Sup35NM (Fig. 3*C*). The reproducibility of the results was confirmed by performing four independent experiments (*SI Appendix*, Fig. S4).

In line with the relatively smaller redshifts in the excitation spectra, the emission spectra of MHB bound to these mutants were redshifted on average 1 nm (Fig. 3*D*). The FWHM of the excitation and the emission spectra of MHB narrowed by 2 nm (Fig. 3*C*), indicating that MHB experienced a more nonpolar environment at these two sites. In contrast, the excitation and emission spectra of MHB in the presence of strong prion fibrils of Sup35NM mutants Y16F, Y29F, Y35F, Y45F, Y49F, Y52F, and Y69F were slightly blueshifted relative to the WT strong prion fibrils (Fig. 3 *G* and *H*). The FWHM for both the excitation and emission spectra of MHB for these mutants broadened by an average of 2 nm (Fig. 3 *G* and *H*). This observation suggests that not only does MHB not bind near amino acids Y16F, Y29F, Y35F, Y45F, Y49F, Y52F, or Y69F in the strong prion fibrils but also MHB experienced a more polar environment in the presence of these mutant prion fibrils than it does when

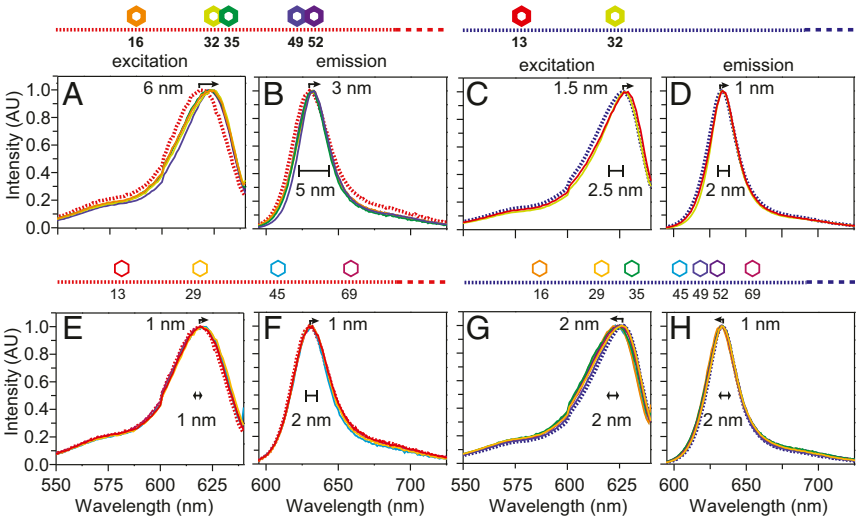

Fig. 3. Normalized excitation (*A*, *C*, *E*, and *G*) and emission (*B*, *D*, *F*, and *H*) spectra of MHB bound to weak (*A*, *B*, *E*, and *F*) and strong (*C*, *D*, *G*, and *H*) prion fibrils. (*A* and *C*) Excitation spectra of MHB in the presence of prion fibrils of Y→F mutants that redshifted compared to the WT Sup35NM prion fibrils (thick dotted lines). (*B* and *D*) Emission spectra of MHB in the presence of prion fibrils of Y→F mutants that redshifted compared to the WT Sup35NM prion fibrils (thick dotted lines). (*E* and *G*) The excitation spectra of MHB in the presence of prion fibrils of Y→F mutants do not redshift compared to the WT Sup35NM prion fibrils (thick dotted lines). (*F* and *H*) Emission spectra of MHB in the presence of prion fibrils of Y→F mutants that do not redshift compared to the WT Sup35NM prion fibrils (thick dotted lines). Spectra with a smaller FWHM have higher unnormalized intensities. The spectra that redshifted also had narrower FWHM (*B*, *C*, and *D*). The unnormalized spectra of MHB in the presence of these mutant prion fibrils had higher intensities than wild-type prion fibrils (*SI Appendix*, Fig. S3).

bound to strong prion fibrils of WT Sup35NM. Our data support multiple binding sites for each unit length of amyloid fibril that is greater for the weak strain than for the strong form. As the conformations are unchanged upon Y→F mutation, the spectral shifts are attributed to a single binding site per unit length.

In contrast to the narrowing of the excitation and emission spectra observed for MHB in more hydrophobic environments, the FWHM of the spectra of ThT bound to the more hydrophobic strong prion fibrils was insensitive to hydrophobicity. This result is reviewed for a subset of the Y→F mutants (*SI Appendix*, Fig. S5). We examined one mutant for each fibril form and found that the Y→F mutation caused redshifts in the excitation spectra but not in the emission spectra of ThT and the FWHM changed by 2% or less, suggesting that ThT is not a particularly sensitive probe.

Taken together, the changes in the excitation and emission spectra of MHB for a single tyrosine to phenylalanine mutation of Sup35NM demonstrate that MHB is capable of detecting small site-specific changes in hydrophobicity.

Discussion

Fluorescent probes are powerful tools to study the assembly of proteins into amyloids. Classic dyes, such as ThT and Congo red, exhibit large increases in fluorescence when bound to extensive β-sheets; however, the excitation and emission spectra of these dyes are not particularly sensitive to local structural or environmental changes that distinguish amyloid polymorphs. As the presence of different polymorphs has been correlated with different phenotypic outcomes, distinguishing between polymorphs and identifying their structural features is important. Some newer dyes such as luminescent-conjugated polythiophenes can distinguish between polymorphs, although the underlying physicochemical rationale is not well delineated and the differences cannot be ascribed to a specific feature. In contrast, the changes in the excitation and emission spectra of MHB in response to changes in polarity are captured by quantum mechanical time-dependent density function theory (31–34). Using two different polymorphic fibrils of Sup35NM, we find that MHB can be used to monitor the assembly of amyloid fibrils of Sup35NM and the fluorescence spectra of MHB distinguish between amyloid polymorphs. MHB is sensitive to both large-scale differences between amyloid polymorphs and small, site-specific changes in local hydrophobicity that result from the conservative mutation of tyrosine to phenylalanine. This result establishes MHB as a dye that can be used to probe both global and site-specific differences in amyloid fibers.

Previous work established that the amyloid core of the weak prion fibrils made from Sup35NM is considerably larger than the amyloid core of the strong prion fibrils of Sup35NM and that the larger amyloid core of the weak prion fibrils is structurally distinct from that of the strong prion fibrils and not simply an extension of a shared common structure (20). The weak prion fibrils have an amyloid core comprising the first 70 amino acid residues. Five mutants of the weak-type Sup35NM prion, in which a tyrosine was replaced with the more hydrophobic phenylalanine (Y16F, Y32F, Y35F, Y49F, and Y52F), had redshifted MHB excitation spectra, a narrowing of the MHB emission spectra, and a decrease in the Stokes shift. These changes indicate that MHB is experiencing a more nonpolar environment. On the one hand, the theoretical calculations support a small redshift in the MHB spectra if a tyrosine at the MHB binding site is replaced with a phenylalanine, which is supported by the experimental observations, suggesting that residues 16, 32, 35, 49, and 52 are located at the binding sites for MHB in weak prion fibrils. On the other hand, the absence of spectral changes, relative to the weak WT prion, of MHB for weak fibrils of Sup35NM in which residues Y13, Y29, Y45, and Y69 were mutated indicates that these residues are not near binding sites for MHB. As all mutated residues fall within the amyloid core of the weak prion fibrils, our findings suggest that these residues are buried and therefore inaccessible to the dye or they are located in regions of local dynamics such as turns rather than in the rigid β-sheets or the unique structural features of individual sites disfavor MHB binding.

The strong prion fibrils had only two MHB binding sites near residues Y13 and Y32. The MHB excitation spectra for strong prion fibrils of these two mutants were redshifted by 1 to 2 nm,

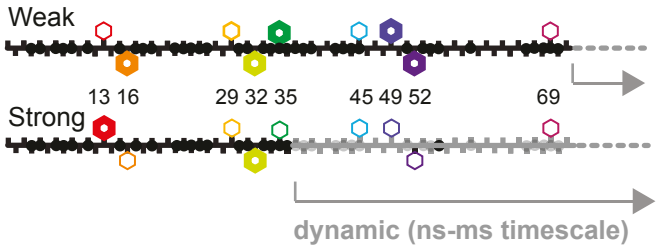

Fig. 4. Schematic folding of the β-sheet-rich regions of weak and strong Sup35NM prions. Single tyrosine to phenylalanine mutations that resulted in spectral shifts for MHB are represented by thick hexagons. Single tyrosine to phenylalanine mutations that did not result in spectral shifts for MHB are represented as thin hexagons. Residues with a backbone amide that was protected from hydrogen–deuterium exchange for a day or more (17) are indicated in black, while backbone amides that were not protected from exchange are shown in gray.

and both the excitation and emission spectra narrowed. These changes indicate that MHB experiences a more nonpolar environment and thus suggest that although the redshift is small, MHB binds at Y13 and Y32 for strong prion fibrils. The relatively modest redshifts could be the result of a different local environment near the amyloid core; the region of the Sup35NM that is sequentially adjacent to the amyloid core is dynamic on the nanosecond to microsecond timescale (20) and may protect the rigid regions from water, making the fibril more nonpolar. Therefore, the smaller redshifts for strong prion fibrils of Y13F and Y32F mutants could be due to the fact that these fibrils present such a hydrophobic environment that excitation and emission spectra of MHB cannot further redshift. For some strong prion mutants there are a blueshift and emission broadening of the MHB spectra relative to the WT, which suggest that the dye experiences a slightly more polar environment. This observation seems at first counterintuitive as the changing from a tyrosine to a phenylalanine should result in a more nonpolar site; however, in the strong-type prions replacing a tyrosine with a phenylalanine could alter dynamics, which could allow the binding site to access water, making the environment more polar.

Several general conclusions can be drawn from the presence or absence of MHB spectral changes observed upon tyrosine to phenylalanine mutation and provide insight into amyloid conformations. If the MHB spectra in the presence of a tyrosine to phenylalanine mutant were redshifted with respect to that of the wild-type protein, then the site of the mutation is located in the rigid amyloid core. While all substituted tyrosine residues are located in the amyloid core of the weak prion fibrils, only half of them are in the amyloid core of the strong prion fibrils, and the ones located in the dynamic region of the strong prion fibrils did not show a redshift in the MHB spectra (Fig. 4). Although these two polymorphs have a shared region in the amyloid core, weak and strong prion fibrils have distinct molecular structures (20, 21). In this shared region, the tyrosine to phenylalanine mutants with redshifted MHB spectra are distinct for the weak and strong prion fibrils. Our findings suggest that the residue Y32 is located in a MHB binding site for both fibril forms, Y16 and Y35 are in MHB binding sites only for the weak prion fibrils, Y13 is in a MHB binding site only for strong prion fibrils, and Y29 is not in a binding site in either fibril form (Fig. 4). The lack of redshift in MHB spectra upon mutation could be due to a variety of reasons, including the fact that the site could be dynamic, located in a turn, or buried and inaccessible to MHB. However, the observation of a redshift in several MHB spectra for prion fibrils upon mutation indicates that the MHB binding site is located in the stable amyloid core and accessible to MHB. Thus, MHB redshifts for tyrosine to phenylalanine mutants highlight site-specific differences in amyloid conformations. There are two regions in Sup35NM where three out of eight consecutive residues are tyrosine residues (Fig. 4). In a continuous β-sheet, the side chains of even and odd residues are displayed on opposite sides. In amyloid fibers, displayed side chains form highly complementary "steric zippers" that exclude water and stabilize interactions between sheets in the amyloid core and tyrosine residues in amyloid core have the same orientation relative to the fibril axis (38), suggesting aromatic ring stacking interaction. Thus, it is notable that for weak prion fibrils, tyrosine to phenylalanine mutants of both Y32 and Y35 as well as Y49 and Y52 have redshifted MHB spectra. This suggests that either MHB can bind to both sides of the β-sheet or there is a turn localized between each of these pairs that would place both tyrosine rings on the solvent-facing side of the amyloid core. Our results support known structural and dynamic differences between these the weak and strong prion strains and provide additional insight into how regions of intrinsic disorder alter the hydrophobicity of the local environment and highlight differences in solvent accessibility of aromatic side chains.

As indicated previously, several parameters can affect the spectral properties of dyes bound to a particular binding site in a β-sheet. MHB is a slightly V-shaped molecule, with C_2 symmetry in planar form, but its two 4-(dimethylamino)phenyl parts also have internal C_2 symmetry, thus allowing only two orientations within a particular binding site. However, despite several attempts during quantum chemical optimization, the second possible binding orientation could not be obtained, indicating that only the currently presented binding orientation is stable (Fig. 2). In contrast, for ThT there are four theoretically possible binding orientations, and all of them could be obtained by the calculations (*SI Appendix*). This will allow a much broader variation of local environmental effects for ThT when compared to MHB, which is in full agreement with the observed differences in FWHM of the spectra for the two dyes (*SI Appendix*, Fig. S1). Furthermore, TDDFT calculations also indicate that when ThT is in a binding mode similar to that of MHB, the Y→F mutation causes a slight blueshift of −1.1 nm for that particular orientation (*SI Appendix*, Table S1).

Changes in accessibility and local environment monitored by spectral shifts can be accomplished in a site-specific manner through the introduction of tyrosine to phenylalanine mutations. Differences in fluorescence spectra observed for bound MHB show that two amyloid fibrils built from Sup35NM have different structures. The sensitivity of the symmetric molecular rotor MHB to the polarity of the environment is now demonstrated by using weak and strong prion fibrils of Sup35NM protein. Considering the amyloid fibrils composed of lysozyme, insulin, and the weak and strong Sup35NM, MHB could distinguish between them by distinct magnitudes in its spectral shifts when bound to various fibrils. The quantum mechanical models derived from previous data on the position of dye molecules bound to fibrils (30, 37) show that MHB could be π-stacked to tyrosine. It is now apparent that MHB not only can distinguish between fibrils made of different proteins but can also point out different conformations of fibrils made from the same protein. As the conservative mutation of tyrosine to phenylalanine can alter the spectroscopic properties of MHB when the site of mutation is located in an accessible region of the amyloid core, MHB can act as a site-specific probe to indicate changes in amyloid structure. This property could be useful to assess structural alterations—potentially in a time-resolved manner—such as amyloid remodeling through the action of chaperone proteins. We anticipate that MHB will be useful for structural understanding of amyloids.

Materials and Methods

Materials. MHB [4,4′-bis(dimethylamino)diphenylmethane] was a gift from the late Dr. Gösta Bengtsson, University of Lund, Lund, Sweden. The synthesis of the dye is described elsewhere (39), and the purity was confirmed

by ^{1}H NMR and gas chromatography–mass spectrometry. A MHB stock solution was made by dissolving the dye in a 10 mM citrate buffer adjusted to pH 4 to give a final concentration of 0.8 mg/mL (1.13 mM). Note that at pH lower than neutral MHB is not present in its uncolored "leuco" (enol) form but in the strongly colored protonated form (Fig. 2*C*).

Strain-Specific Prion Fiber Sample Preparation. The recombinant prion domain of the yeast prion protein Sup35NM was expressed and purified as described elsewhere (18). Tyrosine to phenylalanine mutations were introduced by QuikChange PCR and verified by Sanger sequencing. The protein monomer concentration was determined by ultraviolet/visible (UV/Vis) spectrophotometry using a theoretical extinction coefficient of 25,600 $M^{-1}{\cdot}cm^{-1}$ for wild-type Sup35NM and 24,320 $M^{-1}{\cdot}cm^{-1}$ for single tyrosine to phenylalanine (Y→F) mutants of Sup35NM. Purified Sup35NM in 8 M urea was desalted by the addition of five volumes of methanol, storage at –80 °C, and centrifugation at 4 °C for 10 min at 16,000 × *g*. Methanol-precipitated Sup35NM was recovered as a white pellet and then resuspended and denatured in 6 M guanidine hydrochloride (GdHCl) at 100 °C for 10 min at a concentration around 2 mM. Sup35NM was diluted 400-fold out of 6 M GdHCl in 50 mM potassium phosphate buffer (pH 7.4) and 150 mM sodium chloride. Strain-specific prion fiber samples were prepared by incubation of the denatured Sup35NM monomers at 5 μM with 2% (wt/wt [weight/weight]) of strain-specific seeds at either 4 °C (strong prion fibers) or 37 °C (weak prion fibers) for 2 d. Purified, lysate-templated Sup35NM seeds were prepared from an in vivo prion template as described elsewhere (20, 40), using cell lysates from [*PSI*$^+$] yeast strains exhibiting either the strong or weak prion phenotypes as a template.

Aggregation Kinetics. The amyloid fibril formation by Sup35NM was monitored by ThT and MHB fluorescence measurements. Strain-specific prion fibrillization reactions were prepared by resuspending methanol-precipitated Sup35NM protein in 5% (monomer concentration) solutions of strain-specific seeds and incubation at 25 °C for both strong and weak prion fibrils in 10 mM Tris·HCl (pH 7.4) and 150 mM sodium chloride. The de novo fibrillization reaction was prepared under the same condition but without any strain-specific seeds. The reactions were mixed with the ThT (final concentration of 25 μM) and/or MHB (final concentration of 20 μM) stock solutions. Two hundred microliters of each reaction, in triplicates, were aliquoted onto a 96-well plate. The fibrillization reactions were monitored by fluorescence intensity for either ThT (λ_{em} = 420 nm, λ_{ex} = 480 nm) or MHB (λ_{em} = 595 nm, λ_{ex} = 640 nm). The time-dependent fluorescence intensities were collected on a Tecan Spark plate reader.

MHB Fluorescence Measurements in the Presence of Strain-Specific Sup35NM Fibers. Strain-specific prion fiber samples were prepared by resuspending methanol-precipitated Sup35NM protein in 5% (monomer concentration) solutions of strain-specific seeds and incubation at either 4 °C (strong prion fibrils) or 37 °C (weak prion fibrils) in 10 mM Tris·HCl (pH 7.4) and 150 mM sodium chloride. A 50 μL aliquot of the prion fibrils was mixed with an aliquot of the MHB stock solution, and the sample final volume was adjusted to 1,000 μL with 10 mM citrate buffer (pH 4). Excitation and emission spectra were recorded at λ_{ex} = 580 nm and λ_{em} = 650 nm on a Jobin Yvon-Spex Fluorolog fluorometer using a 1.4 mL volume Hellman quartz cuvette with a path length of 1 cm. The experiments were repeated independently at least three times to ensure reproducibility (the excitation spectra of four independent experiments are shown for the WT, Y13F, and Y29F strong prion fibrils in *SI Appendix*, Fig. S4).

Thermal Stability. Strain-specific Y→F mutant Sup35NM prion fiber seeds were prepared by the addition of 2% (wt/wt) purified, lysate-templated wild-type Sup35NM seeds at either 4 °C (strong prion fibers) or 37 °C (weak prion fibers) for 2 d to purified, denatured solutions of mutant Sup35NM monomer at 5 μM in a 50 mM potassium phosphate buffer (pH 7.4) and 150 mM sodium chloride. Samples for the fiber-melt assay were prepared by templating wild-type Sup35NM monomer from the mutant seeds at 2% (wt/wt) under the prion fiber forming condition described above. The mutant-seeded prion fibril samples were concentrated by centrifugation at 4 °C or 37 °C for 45 min at 16,000 × *g*. The majority (85%) of the supernatant was removed, and each mutant-seeded prion sample was incubated with 2% sodium dodecyl sulphate (SDS) for 15 min at different temperatures (gradient from 25 °C to 95 °C with 10 °C increments). The treated samples were immediately loaded onto a sodium dodecyl sulphate–polyacrylamide gel electrophoresis (SDS/PAGE) gel (Bio-Rad). The bands were quantified by densitometric analysis, and intensities were fit by a sigmoidal model, $y = a + (b - a)/\{1 + \exp[-(x - c)/k]\}$, where a, b, and k are the bottom, top, and slope of the curve and c is the melting temperature of the prion fiber.

Computational Details. The calculations were performed using the Gaussian 09 software package (41). Excited-state energies as well as UV/Vis spectra of MHB and ThT bound to a sheet model were calculated using TDDFT, which was tested for organic dyes (42, 43). Solvent effects of water were considered by using the integral equation formalism polarizable continuum solvent model (IEFPCM) (44). To estimate the effect of Y→F mutation on spectral properties of the dyes when bound to the amyloid fibrils, sheet models containing either Y or F, with bound MHB and ThT, were built by modifying previous quantum mechanical models (30, 37, 45). It was proposed earlier that rod-shaped dye molecules orient parallel to the long axis of the fibrils (30, 37, 46). Current calculations employed a recently developed density functional with dispersion correction, ωB97X-D (47), with the 6-31G(d) basis set (48). Dispersion correction is important for accurate geometry optimization of larger models where dye molecules participate in π-stacking (30, 49), and this functional also includes long-range corrections, or Coulombic attenuation, which was shown to be important for dyes sensitive to the environment to reproduce charge transfer excitations within acceptable accuracy (50). An antiparallel β-sheet model was chosen because lysate-templated prion fibrils do not adopt a parallel-in-register arrangement at the N terminus and other experimental work eliminates models that do not include antiparallel β-strands (51, 52). Optimizations of the antiparallel β-sheet models with one of the bound dyes, MHB or ThT, and either the Y or F residue were performed by using two different ONIOM (our own *N*-layered integrated molecular orbital+molecular mechanics) (53) setups, ωB97X-D/6-31G(d):PM3 and ωB97X-D/6-31G(d):PM3MM, with the dyes and the closer residues on the sheet in the high layer. For MHB both possible orientations relative to the fibril model were considered for optimization, which resulted only in one bound form, while for ThT the orientation which is comparable to that of MHB, with its 4-(dimethylamino)phenyl group stacked to Y or F, was obtained. The optimized geometries were submitted to a total of four TDDFT calculations at the ωB97X-D/6-31G(d):PM3, ωB97X-D/6-31G(d):PM3MM, ωB97X-D/6-31+G(d,p):PM3, ωB97X-D/6-31+G(d,p):PM3MM level of theory, using the IEFPCM model to represent the bulk aqueous environment.

Data Availability. All study data are included in the article and *SI Appendix*.

ACKNOWLEDGMENTS. The late Professor Susan Lindquist was involved in the initiation of this project and the authors acknowledge (and miss) her scientific insight and enthusiasm. King Abdullah University of Science and Technology (Grant KUK-11-008-23) is gratefully acknowledged. We give special thanks to Johan Johansson for assessing the purity of the Michler's hydrol blue sample used in these experiments. Swedish National Infrastructure for Computing resources were used for the quantum mechanics calculations. This work was supported by grants from NSF (Grant 1751174), the Welch Foundation (Grant 1-1923-20170325), NIH (Grant NS-111236), the Cancer Prevention & Research Institute of Texas (Grant RR150076), the Lupe Murchison Foundation, and the Kinship Foundation (Searle Scholars Program) (all to K.K.F.). Support from the Hungarian Academy of Science within the Momentum Programme (Grant LP2016-2) is also acknowledged.

1. M. Sunde *et al*., Common core structure of amyloid fibrils by synchrotron X-ray diffraction. *J. Mol. Biol.* **273**, 729–739 (1997).
2. J. Greenwald, R. Riek, Biology of amyloid: Structure, function, and regulation. *Structure* **18**, 1244–1260 (2010).
3. B. H. Toyama, J. S. Weissman, Amyloid structure: Conformational diversity and consequences. *Annu. Rev. Biochem.* **80**, 557–585 (2011).
4. R. Riek, D. S. Eisenberg, The activities of amyloids from a structural perspective. *Nature* **539**, 227–235 (2016).
5. J. D. Sipe *et al*., Amyloid fibril proteins and amyloidosis: Chemical identification and clinical classification international society of amyloidosis 2016 nomenclature guidelines. *Amyloid* **23**, 209–213 (2016).
6. D. Eisenberg, M. Jucker, The amyloid state of proteins in human diseases. *Cell* **148**, 1188–1203 (2012).
7. T. P. Knowles, M. Vendruscolo, C. M. Dobson, The amyloid state and its association with protein misfolding diseases. *Nat. Rev. Mol. Cell Biol.* **15**, 384–396 (2014).
8. R. B. Wickner, H. K. Edskes, F. Shewmaker, T. Nakayashiki, Prions of fungi: Inherited structures and biological roles. *Nat. Rev. Microbiol.* **5**, 611–618 (2007).
9. J. Shorter, S. Lindquist, Prions as adaptive conduits of memory and inheritance. *Nat. Rev. Genet.* **6**, 435–450 (2005).
10. M. Fändrich *et al*., Amyloid fibril polymorphism: A challenge for molecular imaging and therapy. *J. Intern. Med.* **283**, 218–237 (2018).

11. R. Tycko, Amyloid polymorphism: Structural basis and neurobiological relevance. *Neuron* **86**, 632–645 (2015).
12. K. Annamalai *et al*., Polymorphism of amyloid fibrils in vivo. *Angew. Chem. Int. Ed. Engl.* **55**, 4822–4825 (2016).
13. W. Close *et al*., Physical basis of amyloid fibril polymorphism. *Nat. Commun.* **9**, 699 (2018).
14. A. W. Fitzpatrick *et al*., Atomic structure and hierarchical assembly of a cross-β amyloid fibril. *Proc. Natl. Acad. Sci. U.S.A.* **110**, 5468–5473 (2013).
15. J. L. Jiménez *et al*., The protofilament structure of insulin amyloid fibrils. *Proc. Natl. Acad. Sci. U.S.A.* **99**, 9196–9201 (2002).
16. J. Meinhardt, C. Sachse, P. Hortschansky, N. Grigorieff, M. Fändrich, Abeta(1-40) fibril polymorphism implies diverse interaction patterns in amyloid fibrils. *J. Mol. Biol.* **386**, 869–877 (2009).
17. B. H. Toyama, M. J. Kelly, J. D. Gross, J. S. Weissman, The structural basis of yeast prion strain variants. *Nature* **449**, 233–237 (2007).
18. T. R. Serio, A. G. Cashikar, J. J. Moslehi, A. S. Kowal, S. L. Lindquist, Yeast prion [psi+] and its determinant, Sup35p. *Methods Enzymol.* **309**, 649–673 (1999).
19. M. Tanaka, P. Chien, N. Naber, R. Cooke, J. S. Weissman, Conformational variations in an infectious protein determine prion strain differences. *Nature* **428**, 323–328 (2004).
20. K. K. Frederick *et al*., Distinct prion strains are defined by amyloid core structure and chaperone binding site dynamics. *Chem. Biol.* **21**, 295–305 (2014).
21. R. Ghosh, J. Dong, J. Wall, K. K. Frederick, Amyloid fibrils embodying distinctive yeast prion phenotypes exhibit diverse morphologies. *FEMS Yeast Res.* **18**, foy059 (2018).
22. H. Naiki, K. Higuchi, M. Hosokawa, T. Takeda, Fluorometric determination of amyloid fibrils in vitro using the fluorescent dye, thioflavin T1. *Anal. Biochem.* **177**, 244–249 (1989).
23. H. LeVine III, Quantification of beta-sheet amyloid fibril structures with thioflavin T. *Methods Enzymol.* **309**, 274–284 (1999).
24. M. R. H. Krebs, E. H. C. Bromley, A. M. Donald, The binding of thioflavin-T to amyloid fibrils: Localisation and implications. *J. Struct. Biol.* **149**, 30–37 (2005).
25. V. I. Stsiapura *et al*., Thioflavin T as a molecular rotor: Fluorescent properties of thioflavin T in solvents with different viscosity. *J. Phys. Chem. B* **112**, 15893–15902 (2008).
26. K. P. R. Nilsson, Small organic probes as amyloid specific ligands–Past and recent molecular scaffolds. *FEBS Lett.* **583**, 2593–2599 (2009).
27. J. Orts *et al*., Rational structure-based design of fluorescent probes for amyloid folds. *ChemBioChem* **20**, 1161–1166 (2019).
28. A. K. Schütz *et al*., Binding of polythiophenes to amyloids: Structural mapping of the pharmacophore. *ACS Chem. Neurosci.* **9**, 475–481 (2018).
29. A. I. Sulatskaya, M. I. Sulatsky, I. A. Antifeeva, I. M. Kuznetsova, K. K. Turoverov, Structural analogue of thioflavin T, DMASEBT, as a tool for amyloid fibrils study. *Anal. Chem.* **91**, 3131–3140 (2019).
30. C. C. Kitts, T. Beke-Somfai, B. Nordén, Michler's hydrol blue: A sensitive probe for amyloid fibril detection. *Biochemistry* **50**, 3451–3461 (2011).
31. S. Olsen, Four-electron, three-orbital model for the low-energy electronic structure of cationic diarylmethanes: Notes on a "Pauling point." *J. Phys. Chem. A* **116**, 1486–1492 (2012).
32. S. Olsen, Electronic structure underlying colour differences between diarylmethane dyes and their azomethine analogues. *Aust. J. Chem.* **65**, 520–523 (2012).
33. S. Olsen, R. H. McKenzie, A three-state effective Hamiltonian for symmetric cationic diarylmethanes. *J. Chem. Phys.* **136**, 234313 (2012).
34. S. Olsen, A quantitative quantum chemical model of the Dewar-Knott color rule for cationic diarylmethanes. *Chem. Phys. Lett.* **532**, 106–109 (2012).
35. T. R. Serio *et al*., Nucleated conformational conversion and the replication of conformational information by a prion determinant. *Science* **289**, 1317–1321 (2000).
36. S. M. Uptain, G. J. Sawicki, B. Caughey, S. Lindquist, Strains of [PSI(+)] are distinguished by their efficiencies of prion-mediated conformational conversion. *EMBO J.* **20**, 6236–6245 (2001).
37. C. Rodríguez-Rodríguez *et al*., Crystal structure of thioflavin-T and its binding to amyloid fibrils: Insights at the molecular level. *Chem. Commun. (Camb.)* **46**, 1156–1158 (2010).
38. A. Reymer *et al*., Orientation of aromatic residues in amyloid cores: Structural insights into prion fiber diversity. *Proc. Natl. Acad. Sci. U.S.A.* **111**, 17158–17163 (2014).
39. G. Bengtsson, Polarographic studies of basic triarylmethane dyes. 4. Polarographic behaviour of 2-thiophene green P-methoxy malachite green and crystal violet in aqueous solutions. *Acta Chem. Scand.* **23**, 435–447 (1969).
40. W. N. Costello, Y. Xiao, K. K. Frederick, DNP-assisted NMR investigation of proteins at endogenous levels in cellular milieu. *Methods Enzymol.* **615**, 373–406 (2019).
41. M. J. Frisch *et al*., Gaussian 09 (Revision A.02, Gaussian, Inc., Wallingford, CT, 2009).
42. D. Jacquemin, E. A. Perpète, I. Ciofini, C. Adamo, Accurate simulation of optical properties in dyes. *Acc. Chem. Res.* **42**, 326–334 (2009).
43. J. Fabian, TDDFT-calculations of Vis/NIR absorbing compounds. *Dyes Pigments* **84**, 36–53 (2010).
44. E. Cances, B. Mennucci, J. Tomasi, A new integral equation formalism for the polarizable continuum model: Theoretical background and applications to isotropic and anisotropic dielectrics. *J. Chem. Phys.* **107**, 3032–3041 (1997).
45. A. Perczel, Z. Gáspári, I. G. Csizmadia, Structure and stability of beta-pleated sheets. *J. Comput. Chem.* **26**, 1155–1168 (2005).
46. M. Biancalana, S. Koide, Molecular mechanism of thioflavin-T binding to amyloid fibrils. *Biochim. Biophys. Acta. Proteins Proteomics* **1804**, 1405–1412 (2010).
47. J. D. Chai, M. Head-Gordon, Long-range corrected hybrid density functionals with damped atom-atom dispersion corrections. *Phys. Chem. Chem. Phys.* **10**, 6615–6620 (2008).
48. W. J. Hehre, R. Ditchfie, J. A. Pople, Self-consistent molecular-orbital methods. 12. Further extensions of Gaussian-type basis sets for use in molecular-orbital studies of organic-molecules. *J. Chem. Phys.* **56**, 2257 (1972).
49. M. Matson, N. Carlsson, T. Beke-Somfai, B. Nordén, Spectral properties and orientation of voltage-sensitive dyes in lipid membranes. *Langmuir* **28**, 10808–10817 (2012).
50. D. Robinson, N. A. Besley, P. O'Shea, J. D. Hirst, Di-8-ANEPPS emission spectra in phospholipid/cholesterol membranes: A theoretical study. *J. Phys. Chem. B* **115**, 4160–4167 (2011).
51. K. K. Frederick *et al*., Combining DNP NMR with segmental and specific labeling to study a yeast prion protein strain that is not parallel in-register. *Proc. Natl. Acad. Sci. U.S.A.* **114**, 3642–3647 (2017).
52. R. Krishnan, S. L. Lindquist, Structural insights into a yeast prion illuminate nucleation and strain diversity. *Nature* **435**, 765–772 (2005).
53. T. Vreven *et al*., Combining quantum mechanics methods with molecular mechanics methods in ONIOM. *J. Chem. Theory Comput.* **2**, 815–826 (2006).